Research on surface integrity evolution of short arc assisted milling of superalloy

WANG Pai[1], BAI Yifan[1], ZHAO Wenxiang[2], CHEN Hongtao[1], LIU Zhibing[2,#] and LIU Shuyao[1]

1 School of Mechanical Engineering, Beijing Institute of Technology, Beijing 100081
2 Key Laboratory of Fundamental Science for Advanced Machining, Beijing Institute of Technology, Beijing 100081
Corresponding Author / Email: liuzhibing@bit.edu.cn, TEL: +81-68912716, FAX: +81-68912716

KEYWORDS: Short arc, Recast layer, Surface integrity, Microhardness, Surface strengthening

Short arc milling technology is commonly used in the processing of nickel-based superalloys due to its advantages of low machining stress, cost-effectiveness, and high efficiency. However, the understanding of the evolution of surface integrity in short arc-assisted precision milling is still limited. This study aims to address this issue by analyzing the microstructure characteristics of the recast layer using scanning electron microscopy (SEM), energy dispersive spectrometry (EDS), and other detection methods. Additionally, the influence of precision milling process parameters on surface integrity and the differences in milling surface caused by the presence of the recast layer are investigated through orthogonal milling experiments. The surface strengthening mechanism of short arc-assisted precision milling is also elucidated. The findings reveal that the superalloy crystal undergoes destruction and recombination at high temperatures, resulting in the formation of a recast layer. This recast layer leads to a 34% reduction in hardness and an increase in brittleness. Furthermore, the surface roughness of short arc-assisted milling is found to be larger (Ra=0.76 μm) compared to other milling techniques, and the surface hardening rate is higher (47.8%). Dislocation strengthening is identified as the main factor contributing to surface hardening, and a microhardness change prediction model is developed accordingly.

1. Introduction

Because of their excellent overall qualities, which include exceptional high-temperature strength, good fatigue resistance, and fracture toughness, nickel-based superalloys are frequently employed in the hot-end components of aero-engines [1].

With the quick advancement of special processing technology in recent years, nickel-based superalloys have seen an increase in the use of non-traditional processing techniques to increase production efficiency [2]. The creep fracture was significantly impacted by the oxidation of the recast layer, according to Wen Zhixun's [3] study of the high temperature oxidation behavior of the recast layer of the nickel-based single crystal turbine blade film cooling hole EDM. In his study [4] of the impact of the tool electrode on the superalloy Inconel 825's EDM performance, Saurav Datta analyzed the performance from two angles: material removal effectiveness and electrode wear rate.

Short arc machining [5] is an electrical processing technique that melts and removes metallic or non-metallic conductive materials under the influence of a specific volume of a water-gas mixture working medium at pressure. It not only carries over the benefits of traditional EDM [6], which are not constrained by the material's hardness, strength, or toughness, but also realizes the quick removal of the material.

The method of short arc assisted milling of the nickel-based superalloy GH4169 was employed in this study to examine the microstructure traits of the superalloy's surface following short arc machining. The orthogonal milling experiment was run to examine how surface integrity changed over time. The microscopic elements of the surface strengthening mechanism were investigated.

2. Materials and Machining Process

The chosen material for the test is GH4169, a superalloy, with its main chemical composition listed in Tab.1. The specific processing procedure is illustrated in Fig.1 and can be divided into two stages:

Tab.1 Main chemical composition

Elements	Ni	Cr	Mo	Nb	Ti
Proportion%	51.75	17.00	2.93	5.15	1.07
Elements	Al	C	Si	Mn	Fe
Proportion%	0.45	0.04	0.21	0.03	other

(1) Short arc processing: The blank was processed using a short arc milling machine. A tubular graphite electrode with an outer diameter of 18 mm and an inner diameter of 8 mm was selected. The short arc machining parameters included a discharge voltage of 25 V, an electrode speed of 1500 r/min, a milling depth of 2 mm, and a gas-liquid mixed medium as the working medium. After the short arc machining, the HA400 high-speed wire EDM machine was used to cut the block material, which contained the recast layer, into 9 groups of cuboid specimens with the same size. These specimens have dimensions of 58 mm*15 mm*5 mm and were used as the

experimental group. Additionally, the matrix material was taken, and 9 groups of cuboid samples without a recast layer were obtained using the same wire cutting method as the control group.

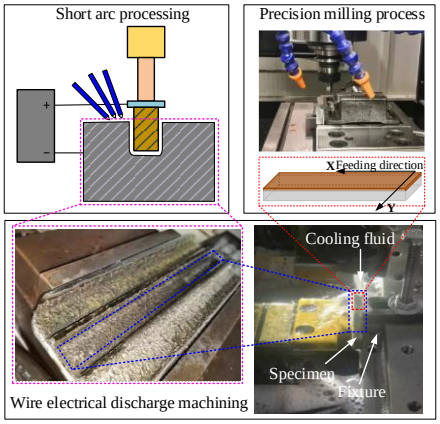

Fig.1 Specific processing process

(2) The precision milling process was conducted on both the experimental and control group using the SMTCL VDM850 CNC machining center. The milling cutter utilized in the test was a customized PCBN unequal tooth pitch 4-edged integral end mill, with a diameter of 16 mm and a cutting edge length of 6 mm. The milling operation was performed in a single pass through end milling. To ensure the accuracy of the test results, a new milling cutter was employed for each specimen. Dry cutting was employed as the lubrication method. The milling parameters were shown in Tab. 2.

Tab.2 Milling parameters

Process	v_c(m/min)	a_p(mm)	f_z(mm/z)
N1	60	0.1	0.04
N2	60	0.15	0.06
N3	60	0.2	0.08
N4	80	0.1	0.06
N5	80	0.15	0.08
N6	80	0.2	0.04
N7	100	0.1	0.08
N8	100	0.15	0.04
N9	100	0.2	0.06

3. Result

3.1 Surface characteristics of recast layer

3.1.1 Microstructure characteristics of recast layer

In order to gain a more detailed understanding of the characteristics of the recast layer at a microscopic level, a study was conducted using wire cutting sampling on the GH4169 recast layer material. The samples obtained from the wire cutting process were subsequently embedded, polished, and corroded through vibration. The samples were then observed using a scanning electron microscope (SEM).

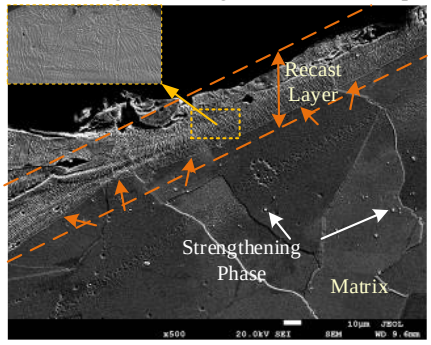

Fig.2 SEM of recast layer and matrix

Fig. 2 illustrates a distinct difference in the microstructure between the GH4169 recast layer material and the matrix material, with a clear demarcation line. At a magnification of 1000 times under the scanning electron microscope, the grain boundary of the recast layer material was not easily discernible, indicating that the microstructure of the high temperature alloy material underwent changes during the process of instantaneous high temperature melting and rapid cooling, resulting in the formation of the recast layer.

3.1.2 Microhardness of recast layer

The MHVS-30AT Vickers hardness tester was employed to measure the distribution of microhardness gradients from the recast layer to the substrate along the depth direction. Fig. 3 illustrates that the center of the indentation of the shallowest sample point is situated approximately 20 μm below the surface of the recast layer, with subsequent sample points being pressed every 40μm along the layer's depth. To mitigate the influence of random error, three points at the same horizontal position were measured, and the average hardness value was selected as the microhardness of the material at that specific position.

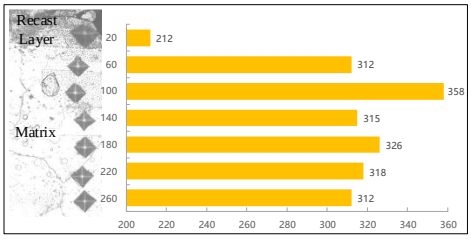

Fig.3 Microhardness changes along the depth direction

The microhardness initially increases, then decreases, and ultimately stabilizes along the depth direction. The reason for the lower microhardness (212 HV) of the recast layer compared to the substrate is primarily attributed to the thermal softening effect during the short arc machining process. The matrix phase of superalloy GH4169 consists of the γ phase, which includes the main strengthening phase γ" phase, the auxiliary strengthening phase γ' phase, δ phase, and carbide [7]. The strengthening phase has a dissolution temperature range of 843-1020 °C. The melting point of GH4169 exceeds 1260 °C. When the recast layer is formed, the instantaneous high temperature surpasses its melting point by a significant margin. Consequently, the original precipitated strengthening phase and grain boundary strengthening phase are completely disrupted, leading to a decrease in microhardness.

3.2 Surface integrity characterization of recast layer milling

3.2.1 Surface morphology

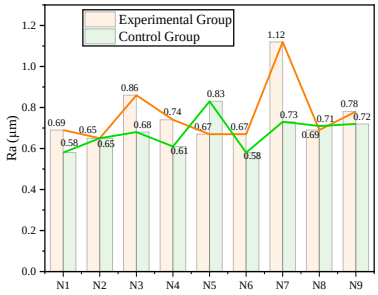

Fig.4 The arithmetic mean deviation Ra of machined surface profile

The evaluation of surface integrity relies heavily on the analysis of surface topography. Fig. 4 presents the arithmetic mean deviation (Ra) of the surface profile for both the experimental and control groups. The

findings indicate that only two groups demonstrate a higher Ra value for the control group compared to the experimental group.

The N7 process is analyzed to determine the maximum difference in Ra between the experimental and control group, as depicted in Fig. 5. It reveals that the experimental group N7 process exhibits a maximum peak-valley difference of 7.76 μm, whereas the control group N7 process displays a maximum peak-valley difference of 5.98 μm. In the 200 μm-600 μm range, the experimental group demonstrates a pronounced milling valley phenomenon, while the control group appears as a nearly horizontal line, indicating a significant disparity. This discrepancy can be attributed to the uneven distribution of material on the surface of the electric erosion and variations in cutting depth during the milling process, leading to tool lifting [8].

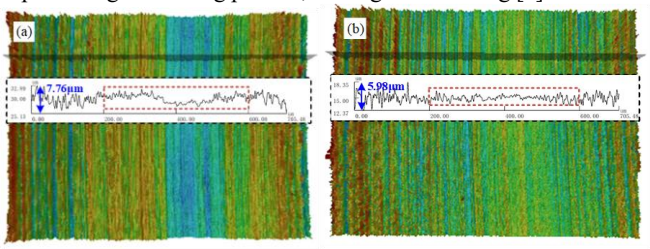

Fig.5 Surface morphology of N7 (a) Experimental (b) Control group

3.2.2 Microhardness

Fig.6 displays the measured microhardness of the experimental and control group. It suggests that the milled surface has undergone noticeable work hardening. Among the nine process groups in the experimental group, N3 demonstrated the highest microhardness, measuring 517 HV, with a surface hardening rate of about 60%.

Comparing the surface microhardness values of the experimental and control group, it was observed that the experimental group generally exhibited higher microhardness values (except for N5, N8, and N9), with an average increase of approximately 24 HV.

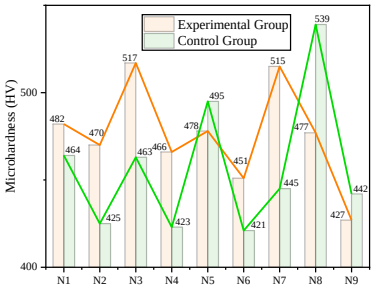

Fig.6 Surface microhardness of experimental and control group

4 Discussion

4.1 Surface crystallographic characteristics

During the milling process of metal materials, the machined surface undergoes complex plastic deformation as a result of severe thermal-mechanical coupling [9]. This plastic deformation causes changes in grain size. To analyze the micro-orientation and grain size on the machined surface, the electron backscatter diffraction (EBSD) technique was employed. The average grain size (diameter) of the surface layer of both the experimental and control group was plotted using the OIM Analysis software, as depicted in Fig.7 (a).

The matrix grain size was found to be 84 μm. The average grain size of the experimental group was measured to be 33.1 μm, while that of the control group was 42.9 μm, with an average grain size difference of 9.8 μm. These findings suggest that precision milling is the primary driving force behind grain refinement.

Kernel Average Misorientation (KAM) is a significant parameter used to measure the local misorientation of crystal materials, which reflects the degree of local plastic deformation. The KAM values of the experimental and control group were determined using OIM software, as depicted in Fig. 7(b). The KAM value of the matrix material was approximately 0.154, while the average KAM values of the experimental (0.293) and control group (0.478) after milling exceeded that of the matrix material. Specifically, the local dislocation proliferation rates of the experimental and control group were 96.8% and 210.6%, respectively. The interaction between the tool and the workpiece resulted in surface crystal twisting and the occurrence of preferred orientation within and between the crystals.

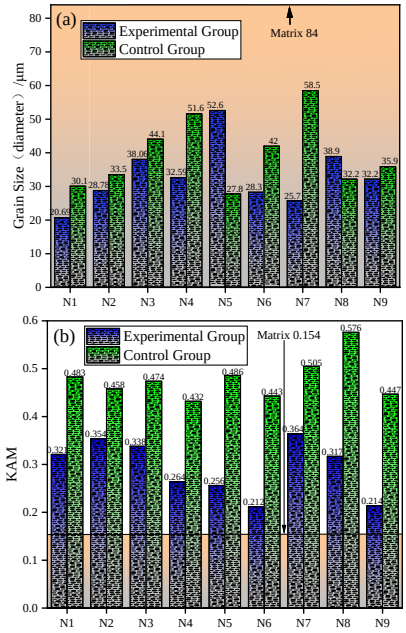

Fig.7 Crystallographic parameters (a) Grain size (b) KAM

4.2 Model of material microhardness change

The prevailing explanation for work hardening is the dislocation theory. Tong [10] suggested that by taking into account the impact of grain refinement and dislocation strengthening on material hardness, it is possible to theoretically predict the hardness of the material.

$$HV = HV_0 + k\frac{1}{\sqrt{d}} + M\alpha Gb\sqrt{\rho} \quad (1)$$

In the given equation, HV represents the local hardness, HV_0 denotes the matrix hardness, k signifies the Hall-Petch constant, d represents the average grain size, M denotes the Taylor factor, α represents a material constant, G signifies the shear modulus, b denotes the length of the Burgers vector, and ρ represents the dislocation density. The formula for calculating ρ is as follows:

$$\rho = \rho_{SSD_s} + \rho_{GND_s} \quad (2)$$

ρ_{SSDs} denote Statistically stored dislocations, and ρ_{GNDs} denote Geometrically necessary dislocations.

The prediction model of material hardness change can be expressed as

$$\Delta HV = k\frac{1}{\sqrt{d}} + M\alpha Gb\sqrt{\rho_{SSD_s} + \rho_{GND_s}} - HV_0 \quad (3)$$

The ρ_{GNDs} can be expressed by the local dislocation difference parameter KAM:

$$\rho_{GND_s} = \frac{2KAM_{ave}}{\mu b} \quad (4)$$

Among them, KAM_{ave} represents the average KAM value of the

selected region, μ is the step size of the EBSD experiment.

The prediction formula of material hardness change is:

$$\Delta HV = k\frac{1}{\sqrt{d}} + M\alpha Gb\sqrt{\rho_{SSD_S} + \frac{2KAM_{ave}}{\mu b}} - HV_0 \qquad (5)$$

To investigate the impact of grain refinement and dislocation strengthening on the microhardness of the machined surface, scatter plots were created and linearly fitted for $d^{-1/2}$-ΔHV, $KAM^{1/2}$-ΔHV, and $GNDs^{1/2}$-ΔHV, as depicted in Fig. 8.

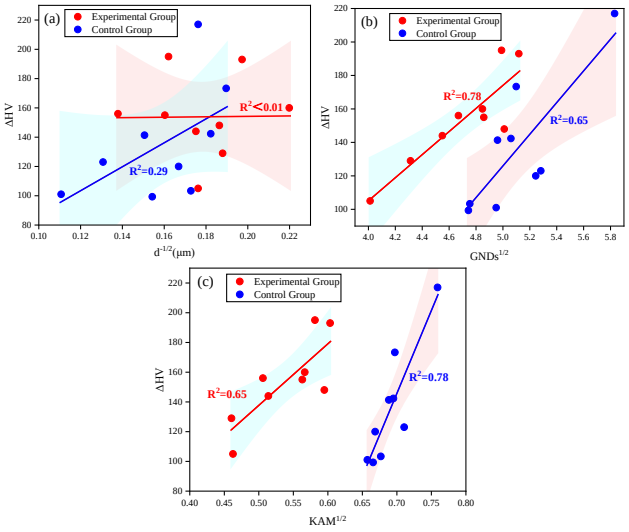

Fig.8 Scatter distribution and linear fitting

The analysis of the image and fitting results reveals that grain refinement does not significantly contribute to surface hardening. Instead, local misorientation and dislocation strengthening resulting from geometrically necessary dislocations are the primary factors.

The fitting results indicate that there is a weak correlation between the change in microhardness (ΔHV) and the grain size ($d^{-1/2}$) in the test group, as evidenced by the close-to-zero linear fitting degree (R^2). Conversely, in the control group, the linear fitting degree is $R^2 = 0.29$, indicating a weak correlation. The heat-affected layer induces changes in grain size beneath the recast layer surface, which superimposes on the grain refinement mechanism resulting from precision milling. Consequently, this weakens the strengthening effect of grain refinement on microhardness and renders it generally irrelevant.

Furthermore, the difference in linear fitting degree between Fig.8(b) and Fig.8(c) demonstrates that $KAM^{1/2}$ exhibits a higher fitting degree than $GND^{1/2}$ in the control group, when not considering the influence of short arc processing. This is because the local misorientation parameter can comprehensively reflect the two parameters of ρ_{SSDs} and ρ_{GNDs}, making it more consistent with the dislocation strengthening mechanism.

5 Conclusion

This paper investigates the evolution of surface integrity in short arc assisted milling of GH4169. The main findings are as follows:

(1) The failure and reorganization of superalloy crystals under the energy field of short arc processing result in the formation of a recast layer, which leads to a 34% reduction in hardness and an increase in brittleness.

(2) The short arc assisted milling surface exhibits a higher average surface roughness of 0.9 μm and an average surface microhardness that is 24 HV higher compared to the conventional milling surface.

(3) The milling process induces significant grain refinement on the surface. However, the contribution of fine grain strengthening to the surface strengthening mechanism is not substantial. Instead, the main factor of surface strengthening is the presence of dislocation strengthening caused by local misorientation and geometrically necessary dislocations.

ACKNOWLEDGEMENT

This work is supported by the National Natural Science Foundation of China (Grant No. 52075042).

REFERENCES

1. Thakur A, Gangopadhyay S. State-of-the-art in surface integrity in machining of nickel-based super alloys[J]. International Journal of Machine Tools and Manufacture, 2016, 100: 25-54.
2. Satish G J, Gaitonde V N, Kulkarni V N . Traditional and non-traditional machining of nickel-based superalloys: A brief review[J]. Materials Today: Proceedings, 2021, 44(1): 1448-1454.
3. Pei H, Wang J, Li Z, et al. Oxidation behavior of recast layer of air-film hole machined by EDM technology of Ni-based single crystal blade and its effect on creep strength[J]. Surface & Coatings Technology, 2021, 419: 127285.
4. Chen Xiaokang, Zhou Jianping, Wang Kedian, Xu Yan. Influence of different tool polarity on short electric arc machining of GH4169[J]. Proceedings of the Institution of Mechanical Engineers, 2020, 234(1-2).
5. Song D, Zhou J, Wang K, et al. Experiment investigation on machining characteristics of 7075 aluminium alloy with short electric arc milling[J]. The International Journal of Advanced Manufacturing Technology, 2021,117: 863-876.
6. Zhou Z, Liu K, Xu Y, et al. Experimental study on high-efficiency DC short electric arc milling of titanium alloy Ti6Al4V[J]. The International Journal of Advanced Manufacturing Technology, 2021,117: 2775-2789.
7. Ren X, Liu Z. Influence of cutting parameters on work hardening behavior of surface layer during turning superalloy Inconel 718[J]. International Journal of Advanced Manufacturing Technology, 2016, 86: 1-9.
8. Hessainia Z, Belbah A, Yallese M A, et al. On the prediction of surface roughness in the hard turning based on cutting parameters and tool vibrations[J]. Measurement, 2013, 46(5): 1671-1681.
9. Dong Z, Xu N, Zhang Y, et al. Mechanism of gradient strengthening layer formation based on microstructure and microhardness of Inconel 718 grinding surface[J]. The International Journal of Advanced Manufacturing Technology, 2022: 2363-2372.
10. Tong Z, Liu H, Jiao J, et al. Microstructure, microhardness and residual stress of laser additive manufactured CoCrFeMnNi high-entropy alloy subjected to laser shock peening[J]. Journal of Materials Processing Technology, 2020, 285: 116806.